#3

HELICAL COUPLING SYSTEM

ALLAN J. LICHTENBERG

TECHNICAL REPORT 290

OCTOBER 6, 1954

RESEARCH LABORATORY OF ELECTRONICS
MASSACHUSETTS INSTITUTE OF TECHNOLOGY
CAMBRIDGE, MASSACHUSETTS

The Research Laboratory of Electronics is an interdepartmental laboratory of the Department of Electrical Engineering and the Department of Physics.

The research reported in this document was made possible in part by support extended the Massachusetts Institute of Technology, Research Laboratory of Electronics, jointly by the Army Signal Corps, the Navy Department (Office of Naval Research), and the Air Force (Office of Scientific Research, Air Research and Development Command), under Signal Corps Contract DA36-039 sc-42607, Project 132B; Department of the Army Project 3-99-12-022.

MASSACHUSETTS INSTITUTE OF TECHNOLOGY

RESEARCH LABORATORY OF ELECTRONICS

Technical Report 290 October 6, 1954

HELICAL COUPLING SYSTEM

Allan J. Lichtenberg

This report is based on a thesis submitted to the Department of Electrical Engineering, M.I.T., 1954, in partial fulfillment of the requirements for the degree of Master of Science.

Abstract

A theory of power coupling between concentric, contra-wound sheath helices has been presented by Kompfner and further amplified by Wade. In Section I of this report a modification of this theory is presented in the light of experimental results, in order to give a more accurate picture of the conditions for complete power transfer from one helix to the other. From the assumption of a sheath helix in free space, a beat wavelength is determined. Correction factors are applied to this result to account for the fact that an actual wire helix is used, and to account for the presence of an environment other than free space. The validity of these correction factors is examined by comparison with experimental results. In Section II the problem of matching a helix to a coaxial line is investigated. A procedure is developed by which the impedance of a helix within a shield may be matched to a coaxial line. With these data and the material developed in Section I, a complete coupling, capable of use on a traveling-wave tube or backward-wave oscillator, is designed and tested.

LIST OF SYMBOLS

V	$-\int E_r\, dr$ voltage on helix
I	helical current
C	capacity of helix to ground
C_{12}	capacity between helix one and two
L	inductance of helix
L_{12}	mutual inductance between helix one and two
Γ	propagation constant along helix considered as transmission line
β	quantity closely related to phase constant of either helix in the Z direction
x	$X_{12}/(X_1X_2)^{1/2}$ normalized mutual reactance
b	$B_{12}/\left[(B_1 - B_{12})(B_2 - B_{12})\right]^{1/2}$ quantity closely related to normalized mutual susceptance
β_b	$\frac{\beta}{2}(x+b)$ beat phase constant
Λ_b	beat wavelength
λ'	wavelength in Z direction along helix
v	phase velocity in Z direction
Z	impedance
c	velocity of light
γ^2	$\beta^2 - \beta_o^2$ radial propagation constant
β_o	free space propagation constant
ψ	helical angle
a	radius of helix
ϵ	dielectric constant of medium
I_o	modified Bessel function for internal problem
K_o	modified Bessel function for external problem
ω	radian frequency
E_z	electric field in z direction
dlf	dielectric loading factor
A	$\frac{\beta_o}{\gamma}\cot\psi$ dispersive factor
b	radius of shield

p	pitch of helix
+	fast wave
-	slow wave
1	inner helix
2	outer helix

INTRODUCTION

The helix has become an important structure for the transmission of electromagnetic energy because of its slow-wave and dispersive properties. It has been used for delay lines, antennas, and more recently, for such tubes as traveling-wave tubes and backward-wave oscillators.

Because of the many uses of a helix as a guide for electromagnetic waves, it has been necessary to devise couplings to transfer power between the helix and more conventional transmission lines. This problem has been complicated for microwave tubes because the helix is in a vacuum, and often at a high dc potential. In such cases direct contact between the helix and conventional transmission systems is difficult to achieve, and usually undesirable.

In the early traveling-wave tubes, this problem was partially solved by use of a waveguide coupling in which the helix served as a probe to excite or pick up energy in a waveguide. A waveguide coupling, however, is inherently a narrow-band device. To take advantage of the wide-band characteristics of traveling-wave tubes and backward-wave oscillators, a broad-band coupling system is necessary. Further restrictions placed on the coupling are that it should be isolated both electrically and physically from the main helix, that the coupling should not add axial length to the helix, and that the region inside the helix should not be disturbed.

Kompfner (1) has demonstrated that power can be coupled between two concentric helices over a broad band. Using this principle, the coupling problem can be divided into two parts: the problem of transferring energy from one helix to the other and the problem of coupling power between a helix and a coaxial line. The purpose of this report is to investigate the possibilities of such a two-stage coupling. Each problem is discussed both theoretically and experimentally; evaluation of the theoretical work is made in the light of the experimental results.

I. HELIX-TO-HELIX COUPLING

1. SPATIAL BEATING OF POWER BETWEEN HELICES

Following the approach of Kompfner (1), Pierce (2), and others, a helix may be considered as a transmission line with a voltage defined as the line integral of the radial field to infinity

$$V = -\int E_r \, dr \qquad (1)$$

and the current taken as the helical current. Considering the lossless case, with a wave variation as $\exp(j\omega t - \Gamma z)$, we can write a set of transmission line equations for the coupling between two helices:

$$\left.\begin{aligned} &\Gamma V_1 - jX_1 I_1 - jX_{12} I_2 = 0 \\ &\Gamma I_1 - jB_1 V_1 - jB_{12}(V_2 - V_1) = 0 \\ &\Gamma V_2 - jX_2 I_2 - jX_{12} I_1 = 0 \\ &\Gamma I_2 - jB_2 V_2 - jB_{12}(V_1 - V_2) = 0 \end{aligned}\right\} \quad (2)$$

This gives us four equations for four unknown voltages and currents. The condition for a nontrivial solution to exist is that the determinant of the coefficients be equal to zero. Solving for Γ and rearranging terms, we have

$$\Gamma^4 + \Gamma^2\left[(B_1 - B_{12})X_1 + (B_2 - B_{12})X_2 + 2X_{12}B_{12}\right] + \left[X_1X_2 - X_{12}^2\right]\left[(B_1 - B_{12})(B_2 - B_{12}) - B_{12}^2\right] = 0 \quad (3)$$

Letting

$$\beta^2 = X_1(B_1 - B_{12}) = X_2(B_2 - B_{12}) \quad (4)$$

and defining quantities

$$x = \frac{X_{12}}{(X_1X_2)^{1/2}} \qquad b = \frac{B_{12}}{(B_1 - B_{12})(B_2 - B_{12})^{1/2}} \quad (5)$$

where x is the normalized mutual reactance, and b is a quantity nearly equal to the normalized mutual susceptance, we can rewrite the expression for Γ in the following form

$$\Gamma^4 + \Gamma^2\beta^2(2 - 2xb) + \beta^4(1 - x^2 - b^2 + x^2b^2) = 0 \quad (6)$$

This expression can be factored to give

$$\Gamma^2 = -\beta^2\left[1 + xb \pm (x+b)\right] \quad (7)$$

which is in the same form as the expression given by Kompfner (1) and Wade (3). This gives us four propagation constants: two for waves traveling to the left and two for waves traveling to the right.

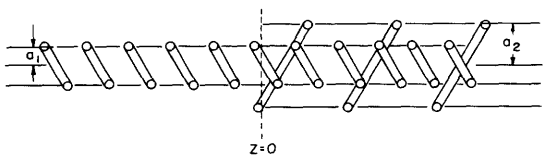

Fig. 1
Cross-wound concentric helices.

Assume a configuration of concentric helices such as that shown in Fig. 1. An equation may be written for the outer helix with the assumption that only two waves are propagating to the right.

$$I_2 = I_2^+ \exp(-\Gamma_1 Z) + I_2^- \exp(-\Gamma_2 Z) \tag{8}$$

$$\Gamma_1 = j\beta\left[1 + xb + (x+b)\right]^{1/2}$$

$$\Gamma_2 = j\beta\left[1 + xb - (x+b)\right]^{1/2} \tag{9}$$

The inner helix is assumed to be of infinite extent in both directions; the outer helix begins at z = 0 and extends to infinity in the positive z direction. Equation 8 will be a valid solution if the boundary conditions can be satisfied.

At z = 0 we have the boundary condition that $I_2 = 0$.

$$I_2^+ = -I_2^- \tag{10}$$

Substituting Eqs. 9 and 10 in Eq. 8 we have the following expression for I_2:

$$I_2 = |I_2|\left[e^{-j\beta\left[(1+xb)-(x+b)\right]^{1/2}z} - e^{-j\beta\left[(1+xb)+(x+b)\right]^{1/2}z}\right] \tag{11}$$

Equation 11 describes two waves of the same amplitude traveling in the same direction at different phase velocities. These waves will beat spatially with a periodicity depending on the values of x and b. If x and b are equal, the quantities under the radical become perfect squares, and I_2 immediately reduces to

$$I_2 = |I_2|\, e^{-jbz} \sin\frac{\beta}{2}(x+b)z \tag{12}$$

For x and b << 1 a power expansion of the square roots can be used, giving

$$I_2 = |I_2| \exp\left[-j\beta\left(1+\frac{xb}{2}\right)z\right] \sin\frac{\beta}{2}(x+b)z \tag{13}$$

or, ignoring the second-order term in x and b, we have

$$I_2 = |I_2|\, e^{-j\beta z} \sin\frac{\beta}{2}(x+b)z$$

which is the same as Eq. 12. This represents a standing wave on the outer helix with the envelope phase constant given by

$$\beta_b = \frac{\beta}{2}(x+b) \tag{14}$$

and a wavelength

$$\Lambda_b = \frac{2\lambda'}{x+b} \qquad \left(\lambda' = \frac{2\pi}{\beta}\right) \tag{15}$$

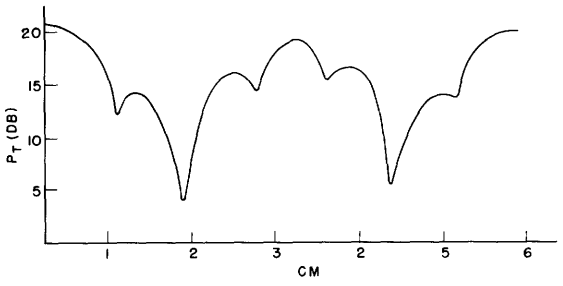

Fig. 2
Transmitted power vs. interaction distance.

Since we have assumed only two waves traveling in the positive z direction in order to achieve this solution, the energy must be spatially beating from one helix to the other. If conditions are such that the voltage and current are in phase on the outer helix, all of the power will beat between the two helices as $\cos^2 \beta_b z$. These conditions will be discussed in Section I-2.

If the two helices interact for exactly one quarter of a beat wavelength, the power will be completely transferred from one helix to the other. Power will be reflected for interaction distances other than an odd multiple of quarter-beat wavelengths.

An experimental plot of power transmitted vs. interaction distance is given in Fig. 2. The beat character is quite clear, with the sharp minima coming at interaction distances of $\Lambda_b/2$. The broad maxima and sharp minima can be explained quite easily in terms of multiple reflections within the coupling (4).

2. CONDITIONS FOR COMPLETE POWER TRANSFER

a. Strong and Weak Coupling

The beat wavelength was shown to be given by

$$\Lambda_b = \frac{2\lambda'}{x + b} \tag{15}$$

If x and b are of equal or nearly equal magnitudes, there will be two coupling conditions: strong coupling for x and b of like signs, and weak coupling for x and b of unlike signs.

For two concentric helices, Pierce (2) has shown that the charge build-up on one helix caused by a positive voltage on the other, is opposite in sign to the charge build-up caused by its own positive voltage. For this reason, a negative sign may be affixed to C_{12}. Since we do not usually like to speak of negative capacities, the same result might more logically be achieved by a sign change in Eqs. 2. In either case, the end result is to give a negative sign to b. To achieve strong coupling, it is therefore necessary to have x also negative. As it was pointed out by Pierce, this can be achieved by winding the helices with opposite senses. Since the strongly coupled case is the practical

one, the work reported here, both theoretical and experimental, considers only oppositely wound helices.

b. Phase Velocity Condition

To separate the determinantal expression for Γ into four propagation constants, two of which travel in the positive z direction and two of which travel in the negative z direction, it is necessary to let

$$X_1(B_1 - B_{12}) = X_2(B_2 - B_{12}) \tag{4}$$

This immediately gives us a condition between the phase constants of the two lines

$$X_1B_1 - X_2B_2 = B_{12}(X_1 - X_2) \tag{16}$$

By using the relations

$$v = \frac{1}{(LC)^{1/2}} \qquad Z = (L/C)^{1/2} \tag{17}$$

and with a little manipulation, an equation relating the phase velocities is obtained

$$v_2^2 = v_1^2 \left[1 + \frac{b(Z_1 - Z_2)}{Z_{mean}}\right] \tag{18}$$

Both b and Z will be shown to be calculable quantities by which a fairly precise measure can be obtained for the difference in phase velocities between the two helices.

In practice, for two concentric helices with an outer shield, Z_1, the impedance of the inner helix, is larger than Z_2, the impedance of the outer helix. Since b has been given a negative sign by an argument presented earlier, the phase velocity of the inner helix is slightly greater than that of the outer helix. Since b is usually a small number, and Z_1 is not too different from Z_2, one might be tempted to let $v_2^2 = v_1^2$. This has been done by most authors by ignoring certain terms in the original differential equations. While this simplified condition leads to reasonable results, it has been pointed out by Wade (3), Lacy (5), and Stark (6) that the condition for complete transfer of power is critically dependent on the phase velocity. One can, in fact, achieve much better coupling by making the phase velocities slightly different by use of Eq. 18. This increase in power transfer in the forward direction can best be seen by examining the directivity of the coupling, that is, the ratio of forward to backward power.

Directivity experiments showing this effect were first made by Stark at a relatively low frequency. He was able to better his directivity by as much as 10 db by experimentally changing the velocity of one helix from the equal phase velocity condition until a maximum directivity was obtained.

This author, working at a higher frequency, between 2 kMc and 6 kMc, experimentally compared the directivities of two couplings, one with equal phase velocity helices, and one with phase velocities computed from Eq. 18. The directivity plots of these two

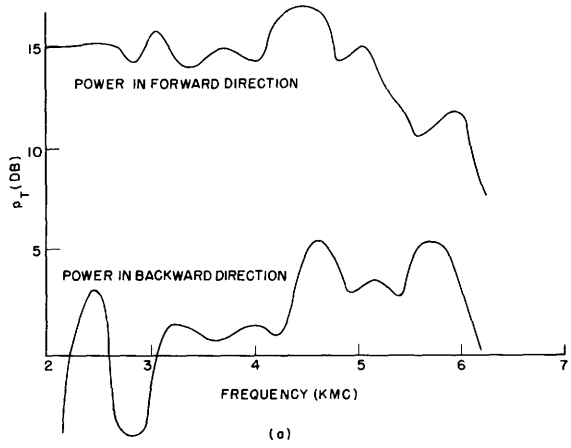

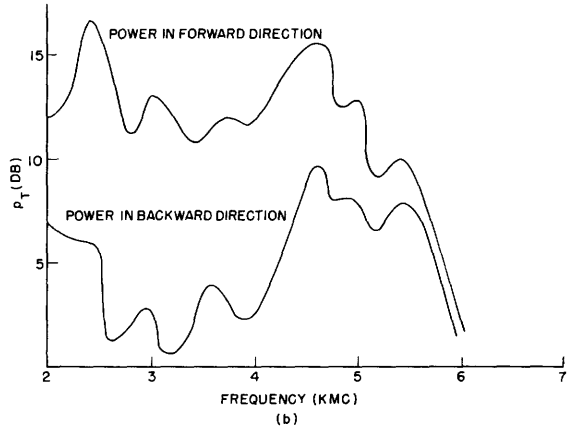

Fig. 3

Directional properties of coupler (a) with correct phase velocity: $v_2 = v_1 \left(\frac{1+b(Z_1-Z_2)}{Z_{mean}} \right)^{1/2}$; (b) with $v_2 = v_1$.

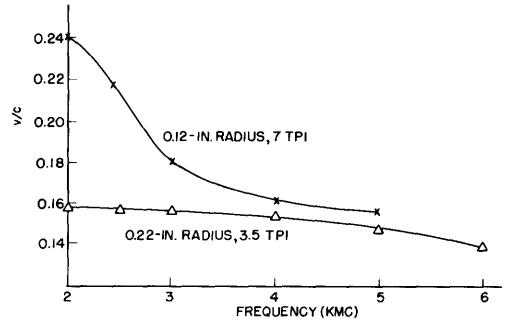

Fig. 4

Phase velocities of inner and outer helices in coupling.

couplings are compared in Fig. 3. For the conditions of coupling used (described more fully later), the difference in phase velocity for maximum coupling was found to be 4.5 $\pm$ 0.5 per cent. The experimental helices were made to these specifications with an experimental tolerance of $\pm$ 1 per cent.

Because the phase velocity condition is extremely critical, the velocities of the helices must be determined very accurately. In an actual traveling-wave tube the presence of dielectric and outer shield makes a theoretical determination of these phase velocities quite difficult. Measurements, however, are quite easy to perform. A complete description of the method is given in the appendix. The relative phase velocities of two helices are plotted in Fig. 4. They were adjusted to give a 4.5 per cent faster velocity on the inner helix at 4 kMc. This was done in accordance with the theoretical determination for the difference in velocities to give the optimum power transfer.

The graph of Fig. 4 demonstrates another important point: the phase velocities of two helices of different cross section can only be matched at one particular frequency. The small-diameter helix becomes more dispersive at low frequencies, since its $\beta_o a \cot \psi$ is only a little over half that of the large-diameter helix. Another reason for the smaller dispersion of the outer helix lies in the presence of the outer shield. Mathers and Kino (7) have calculated the dispersive characteristics of a helix inside a shield. This graph is given in Fig. 5. Figure 5 will also be used in Section II to determine the impedance of a helix in a shield.

A question must now be raised. How can a pair of helices be chosen that will give optimum performance over the entire range desired? One would intuitively feel that some sacrifice of performance in the midband region would probably be necessary for maximum over-all performance. In the actual directivity experiments performed, the directivity was better at lower frequencies than at the midband frequency. This is probably the result of an underestimation in the difference in impedances Z_1 and Z_2 that were used to calculate the phase velocities. In Section II the impedance question will be taken up in more detail when the general impedance properties of a helix within a shield are discussed.

c. Conditions on x and b

It has been shown that if, for two coupled helices that meet the phase velocity condition, the current (or voltage) on one helix goes to zero somewhere, it will periodically go to zero along the line. To show that energy is completely transferred from one helix to another, it must also be shown that current going to zero on one helix implies both current and voltage going to zero on both helices. These conditions will be satisfied if

$$\frac{I_2^+}{I_1^+} = \frac{I_2^-}{I_1^-} \tag{19a}$$

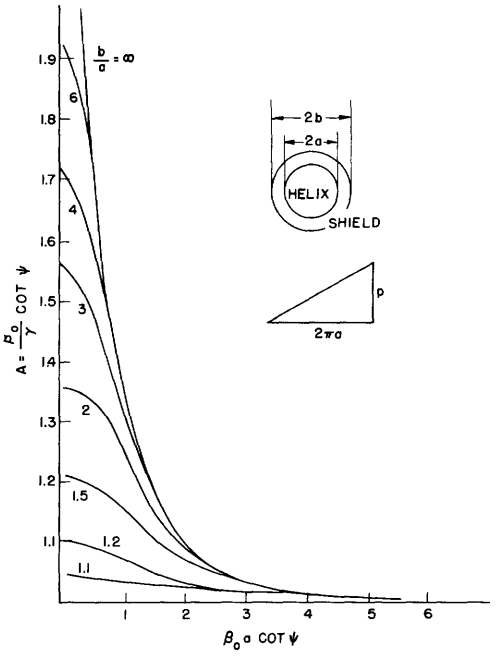

Fig. 5

Dispersion characteristic of a shielded helix.

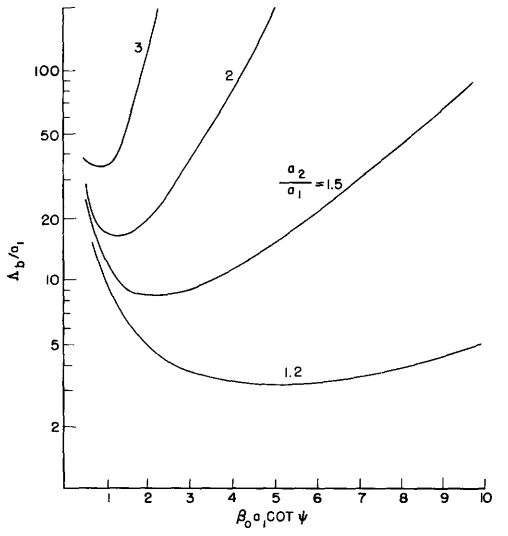

Fig. 6

Beat wavelength using sheath helix approximation.

and

$$\frac{I_2^+}{V_2^+}=\frac{I_2^-}{V_2^-} \tag{19b}$$

where the plus and minus signs stand, respectively, for the fast and slow waves. Solving for these ratios from Eqs. 2, it is found that the first is satisfied automatically, and that the second is satisfied for

$$x, b \ll 1$$

$$x \simeq b \tag{20}$$

No direct experimental evidence was obtained to substantiate this theory. In the experiments of power transmission, x and b were probably changed independently by varying dielectric surroundings. For the small coupling coefficients used, however, any changes in coupling coefficients were masked by more critical phase velocity changes.

3. DETERMINATION OF THE BEAT WAVELENGTH

a. Helical Sheath Model

The beat wavelength was previously defined as

$$\Lambda_b = \frac{2\lambda'}{x + b} \tag{15}$$

As it was pointed out in the discussion of phase velocities, λ' can be determined quite easily by experiment. The quantities x and b remain to be determined.

Pierce has suggested that for two helices in free space, a simple ratio of fields may be used to determine the coupling coefficients.

$$x^2 = b^2 = \frac{E_1(\gamma a_2)\, E_2(\gamma a_1)}{E_1(\gamma a_1)\, E_2(\gamma a_2)} = \frac{K_o(\gamma a_2)\, I_o(\gamma a_1)}{K_o(\gamma a_1)\, I_o(\gamma a_2)} \tag{21}$$

where $\gamma^2 = \beta^2 - \beta_o^2$, and the subscripts 1 and 2 refer to the inner and outer helices, respectively. This expression has been justified by Wade (3) and by the author (4). In Fig. 6, Λ_b is plotted against $\beta_o a_1 \cot \psi$ for values of a_2/a_1 that might be used in a practical coupling.

The experimentally determined beat wavelength was considerably larger than the one calculated from the sheath helix coupling coefficients. For this reason correction factors must be applied in order for us to determine the correct beat wavelength. The sheath helix model, however, can be used by itself to obtain much useful information. An examination of Fig. 6 shows that a helix-to-helix coupling is a very broad band device. If parameters are so chosen that at the midband operating frequency the value of Λ_b is a minimum, the beat wavelength changes very slowly with changes in frequency. Combining this with the transmission characteristics of Fig. 2, it can be seen that for the helices used the power transmitted was down less than 2 db an octave on either side of the midband frequency.

Because of the desirability of choosing parameters so that the minimum beat wavelength is at the midband frequency, it is necessary to relate the propagation constant β to the physical dimensions of the two helices. By expanding the expression for β_b in terms of the Bessel functions of large arguments, and maximizing in respect to β, we find that

$$\beta = \frac{1}{a_2 - a_1} \tag{22}$$

If at the midband frequency, β and a_1 are fixed by outside conditions, the radius of the coupling helix a_2 can be adjusted within certain limits to fulfill the desired condition.

A restriction on a_2, which is interdependent with the maximum operating frequency of the coupling, is given by the cut-off frequency of the coupling helix. From Sensiper's (8) analysis the inequality

$$|m| + \frac{\beta_o a}{\cot \psi} < \frac{\beta a}{\cot \psi} < |m| - \frac{\beta_o a}{\cot \psi} \tag{23}$$

where $\beta > \beta_o$, and $|m| \geq 1$ (m is any integer), must be satisfied for a given helix to be

in a propagating region. From this inequality we can obtain a condition on λ for the helix to be in a propagating region.

$$\lambda > 2\pi a(1 + \sin \psi) \tag{24}$$

This gives the minimum wavelength for a given helix radius, a.

The coupling helices used experimentally had radii of 0.22 inches, and sin ψ was approximately 0.2, giving a value of 4.2 cm for λ, or a frequency of 7.1 kMc. If the dispersiveness of the helix is taken into account, Eq. 24 is modified to

$$\lambda > \frac{2\pi a(1 + \sin \psi\, d)}{d} \tag{25}$$

where d is the dispersive factor; for a d of 0.8, the cut-off frequency is reduced to 6.4 kMc. Above this frequency the entire derivation for power transfer is no longer valid. This should manifest itself in a sharp decrease of transmitted power.

In Fig. 7 a typical experimental plot of power transmitted in the forward direction is given between 2 kMc and 7 kMc. The transmitted power begins to fall off at a lower frequency than that predicted. Standing-wave-ratio-measurements also indicate a sudden rise in reflected power between 5.4 kMc and 5.6 kMc. The reason for this early drop-off is not clear. It does indicate though, that the value of a_2 should be kept small enough so that the upper operating frequency is still well below cutoff. As mentioned earlier, this may entail some compromise with the condition that a_2 should be so chosen that the minimum beat wavelength be located near the midfrequency of operation.

The preceding analysis has given a picture of the operation of the beat wavelength and the transfer of power. However, as it was mentioned earlier, an accurate calculation of the beat wavelength for a practical coupling cannot be made from this simplified model. To make an accurate calculation, the effects of the dielectric and the outer shield, and the effect of the use of a real wire helix rather than a sheath helix will have to be considered. These factors will be taken into account in the following sections.

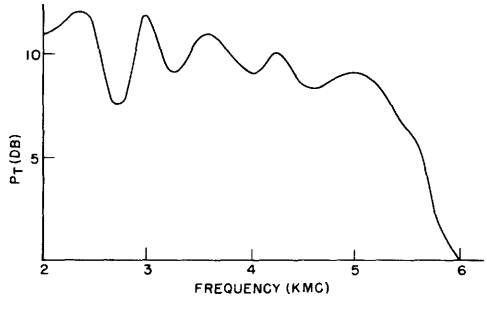

Fig. 7

Power transmitted by coupling, showing relative power at frequencies of interest.

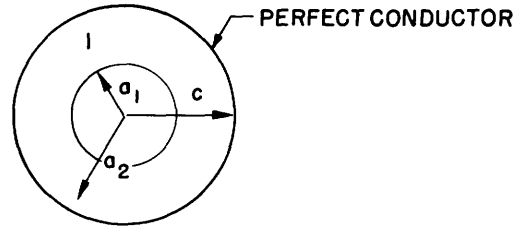

Fig. 8

End view of helix and coupling geometry.

b. Effect of Outer Shield

To determine the effect of a shield, a good approximation to the fields may be obtained by a quasi-static approach. If a simple sinusoidal field distribution with the correct periodicity is assumed at the helix radius, the E_z fields are equivalent to those for the helix. The geometry considered is shown in Fig. 8. Helix 2 would be between the inner helix and the shield at a radius a_2. The boundary conditions are

$$E_1(\gamma a_1) = \sin \gamma z$$

$$E_1(\gamma c) = 0 \tag{26}$$

The general solution in region I is

$$E_1 = \left[AI_o(\gamma r) + BK_o(\gamma r)\right] \sin \gamma z \tag{27}$$

A and B may be evaluated from Eq. 26. The ratio of the fields at the two helices may then be determined.

$$\frac{E_1(\gamma a_2)}{E_1(\gamma a_1)} = \frac{AI_o(\gamma a_2) + BK_o(\gamma a_2)}{AI_o(\gamma a_1) + BK_o(\gamma a_1)} \tag{28}$$

This can be compared with the ratio without the outer conductor present. The ratio of the fields caused by helix 2 remains the same. The increase in beat wavelength can then be computed from Eqs. 21 and 15. This computation was carried out for $a_1 = 1.63$, $a_2 = 2.98$, and $c = 4.14$, which were the radii of the experimental helices and shield. A 7 per cent increase in beat wavelength was calculated; it agreed quite closely with that found by experiment. In Figs. 9 through 11 this increase in Λ_b is plotted for various values of γa.

c. Effect of Dielectric

The presence of a dielectric in the vicinity of a coupling has two effects: it changes the phase velocity of the individual helices, and it changes the over-all field configuration between the helices. The first effect increases the longitudinal propagation constant β, and therefore changes the place of operation on the Λ_b vs. βa_1 curve. This change can be computed from the change in phase velocity resulting from the dielectric loading that was experimentally determined. The new βa_1 is defined as the product of $\beta_o a_1 \cot \psi$ and the dielectric loading factor (dlf). Any small changes in phase velocity resulting from the presence of the shield may be lumped together with this factor.

The second effect can be treated by a quasi-static approach similar to that used for the outer shield. The situation is somewhat more complicated since the boundary conditions for three regions rather than one must be satisfied. This computation was carried out, giving a theoretical increase in Λ_b. Experimentally, however, this increase was not observed, probably because there is a canceling effect from higher harmonics. This factor will be discussed in the next section.

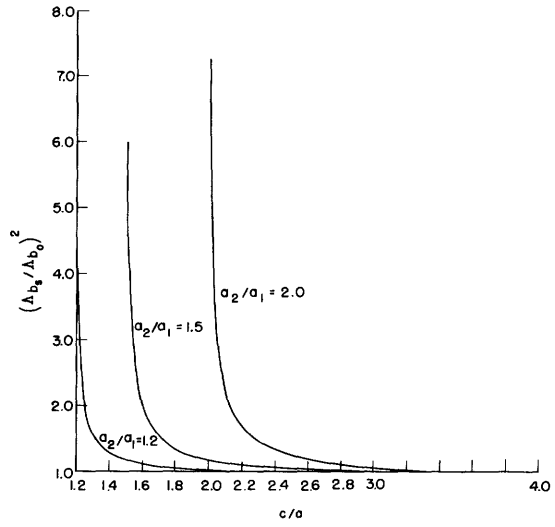

Fig. 9

Increase in beat wavelength in the presence of a shield; $\gamma a_1 = 1$.

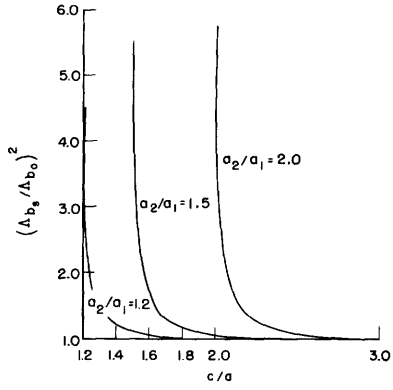

Fig. 10

Increase in beat wavelength in the presence of a shield; $\gamma a_1 = 2$.

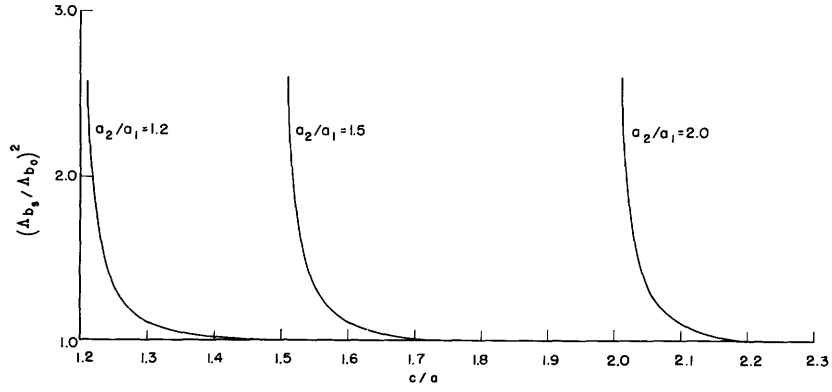

Fig. 11

Increase in beat wavelength in the presence of a shield; $\gamma a_1 = 8$.

d. Effect of a Real Wire Helix

Assume a sinusoidal distribution of potential on a cylinder replacing the helix, as in the preceding section. If this potential exists only in regions where there is an actual wire, as shown in Fig. 12, the potential function can be represented as a Fourier series of period p, and modulated by an envelope of cos γz.

$$\sum_{n=0}^{\infty} a_n \cos\left(\frac{2\pi n}{p} z\right) \cos \gamma z \tag{29}$$

By the use of a trigonometric identity this may be transformed to

$$a_o \cos \gamma z + \sum_{n=1}^{\infty} a_n \cos\left(\gamma \pm \frac{2\pi n}{p}\right) z \tag{30}$$

Equation 30 gives the expression for the fundamental, and the higher order space harmonics caused by the periodicity of the structure. These harmonics also carry power and couple between the two helices. They are not independent, however, since a change in amplitude of one must change all of the others. A general solution to this problem would entail the solution to the interaction between each harmonic separately, and then the solving of the n^{th} order perturbation problem between them. The zeroth order approximation (each harmonic coupling independent) gave an increase in beat wavelength considerably smaller than that observed by experiment.

Experimentally, the beat wavelengths of three helix combinations were found for varying diameter ratios. As predicted from the theory stated above, the higher harmonic interaction had more effect in lengthening the beat wavelength when the helices were closely spaced. This is because the higher harmonic amplitudes drop off much more rapidly with distance than the fundamental amplitudes. In Fig. 13 the experimentally determined Λ_b for real wire helix combinations are compared with the sheath helix counterparts. Comparisons were made at the midband frequency for each coupling.

The experimental beat wavelength was determined by noting the power transmitted from one helix to another as the helix interaction distance was changed. A second periodicity was noted at the helical wavelength. This periodicity was, surprisingly, more marked for the larger helix spacings. The cause of this secondary effect has not been explained.

II. HELIX-TO-COAXIAL-LINE COUPLING

1. IMPEDANCE MATCHING

In Section I, the problem of coupling power from one helix to another was discussed in detail. This essentially solves one half of the traveling-wave tube or backward wave oscillator coupling problem: that of transferring power between a helix in an evacuated

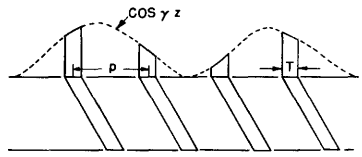

Fig. 12

Schematic of voltage wave on real periodic helix.

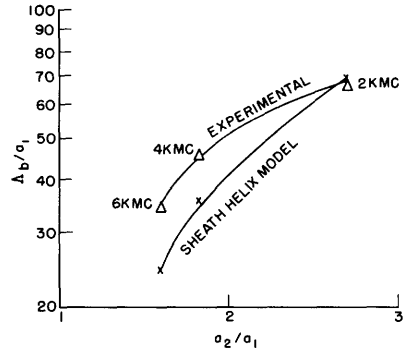

Fig. 13

Comparison of beat wavelength by experiment and by sheath helix calculations.

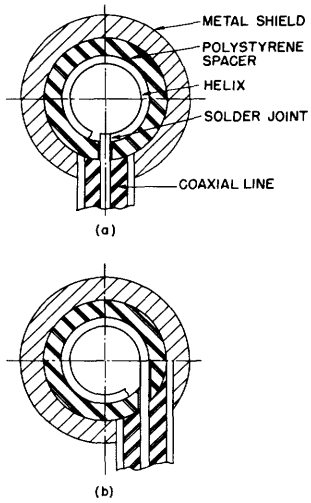

Fig. 14

End view of helix-to-coaxial-line coupling: (a) perpendicular entry; (b) tangential entry.

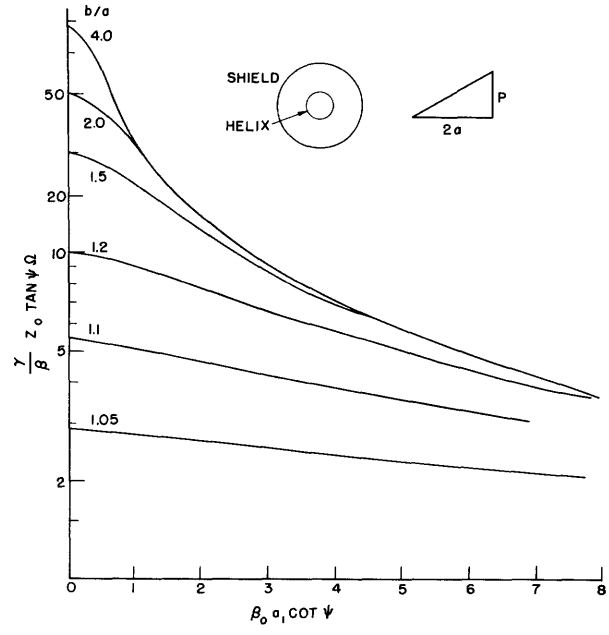

Fig. 15

Impedance parameter for a helix in a shield.

tube and the outside world. The second part of the problem, that of coupling between a helix and a conventional transmission system, remains to be discussed. Because of its wideband characteristics, a coaxial line was used as the external transmission system.

In order to match one system to another, impedances must be matched either directly or through a transformer, and a smooth transition of fields must be made at the juncture. Beside this general matching problem, the condition of not adding axial length to the structure should also be considered. The types of transition chosen for experiment are shown in Fig. 14.

In Fig. 14(a) the helix is perpendicular to the center conductor of the coaxial line at the solder connection. In Fig. 14(b) the helix is tangential to the center conductor of the coaxial line at the solder connection. The advantages of a perpendicular entry coupling are that it is easier to build, and that probably there is a smaller region where the impedance is different from that of the helix in a shield or that of the coaxial line. The advantage of the tangential entry is a much smoother transition, with a proportional decrease in the field distortion.

In practice, it was found that for any given shield the tangential entry gave considerably less reflected energy when averaged over the frequency band tested. Because of this result, the tangential entry will be considered in all subsequent discussions.

The main problem, however, is matching the high impedance helix to a low impedance coaxial line. One method of accomplishing this is by surrounding the helix with a shield. The general problem of a real helix inside a shield has not yet been solved in detail, but approximate methods, which lead to useful results, may be used.

Mathers and Kino (7) solved the problem for the impedance of a sheath helix inside an outer conductor, using as a definition of impedance

$$P = \frac{1}{2} Z_o \, I \, I^* \tag{31}$$

where I is the current on the helical sheath, and P is found by integrating the Poynting vector over the area within the shield. The results of their calculations are reprinted in Fig. 15.

In order to take into account the presence of the dielectric, Mathers' original expression for Z_o must be examined.

$$Z_o = \frac{\beta}{\beta_o 4\pi} (\mu/\epsilon)^{1/2} \frac{I_o^2(\gamma a)}{I_o^2(\gamma b)} (\gamma a)^2 D^2(\gamma a, \gamma b) \tag{32}$$

where $D(\gamma a, \gamma b)$ is a complicated function of the Bessel functions. As ϵ increases, Z_o is reduced in two ways: first, by the $\epsilon^{1/2}$ in the denominator; second, by the increase in the propagation constant β_o caused by the presence of the dielectric. This impedance reduction caused by the increase in β_o can easily be seen from Fig. 15. For an actual

impedance calculation, the dielectric loading factor rather than $\epsilon^{1/2}$ should be used to obtain the correct impedance reductions. The dielectric loading factor itself was obtained accurately from the phase velocity measurements discussed in Section I, but could be approximated from work done by Smullin and associates (9). One factor mentioned above should be emphasized: the helix impedance changes with β_o. This means that the Z_o of the helix can only be exactly matched to the coaxial line at one frequency. For closely spaced shields, the impedance is fairly constant. As will be shown later, however, experimental results with closely spaced shields gave unsatisfactory results.

A good low frequency approximation, when the helix-to-shield spacing is quite close, as compared to the other helical dimensions, is the wire above ground plane, shown in Fig. 16. By a simple electrostatic calculation, Z_o is known to be

$$Z_o = \frac{60}{\epsilon^{1/2}} \cosh^{-1} \frac{2h}{d} \tag{33}$$

By comparison with a model of a real wire helix in a shield at low frequencies, developed by Kirschbaum (10), this approximation is found to be satisfactory up to quite large helix-shield spacings.

From static considerations one would expect the sheath helix model to give lower impedances at all frequencies than a real wire helix. As the frequency increases, the impedance of a real helix would have to drop off in a manner similar to the impedance drop-off of the sheath helix while always remaining above it. To obtain a complete picture of the real helix at all frequencies, it is only necessary to give Z_o the value of the line above ground at low frequencies, and as the frequency increases have Z_o decrease proportionately to the decrease of the sheath helix impedance. In Fig. 17 the calculated impedance vs. frequency characteristic is plotted for the three shields used experimentally. For all cases the dielectric loading factor was taken as 1.38, the sine of the helical angle as 0.207, the mean diameter of the helix as 0.44 inch, and the diameter of the wire as 0.04 inch.

A large quantity of experimental data was obtained in an attempt to verify the theoretical results. Voltage-standing-wave measurements were taken with a coaxial slotted line, joined by type N connectors to the coaxial line attached to the helix and sheath combination. A glass tube inside the helix was given a graded Aquadag coating to make it serve as a matched termination. Typical early measurements with a fairly long piece of cable between the slotted line and the shield are given in Fig. 18. The 0.610-inch and 0.750-inch (inside diameter) shields were used, the more closely spaced shield giving the better results. The rapid variations of voltage-standing-wave ratio (VSWR) were interpreted as cable resonances between the discontinuity at the helix-coaxial junction and the connector at the slotted line. The period of the fluctuation corresponded roughly with the distance necessary for a 360° phase change between the ends of the line. The frequency of the oscillation did increase with the applied frequency, but not as rapidly as it should have if this were the complete explanation.

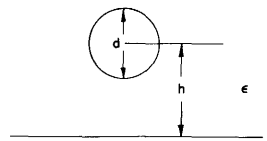

Fig. 16
Line above ground plane geometry.

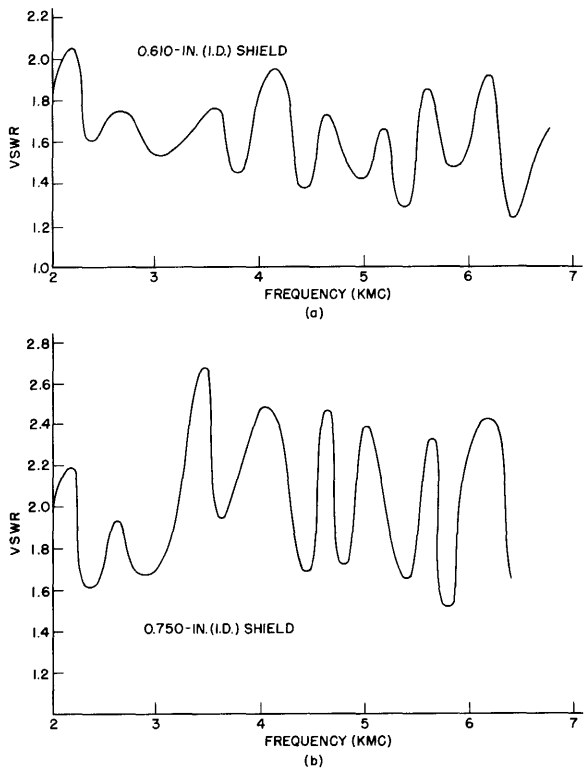

Fig. 18
Comparison of voltage-standing-wave ratios: (a) 0.610-inch (I.D.) shield; (b) 0.750-inch (I.D.) shield.

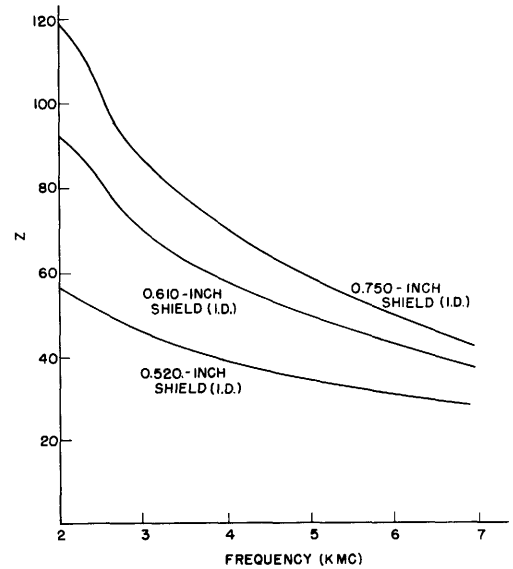

Fig. 17
Calculated theoretical impedances of helix in three different shields.

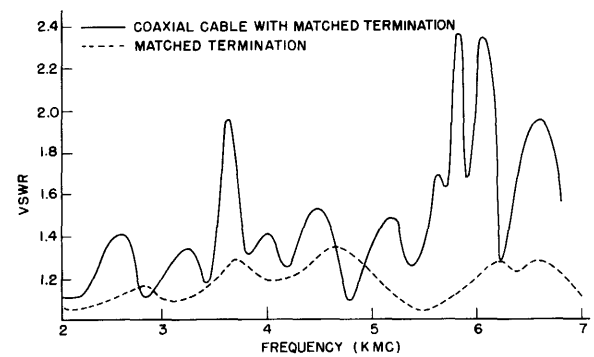

Fig. 19
Control measurements.

Standing-wave measurements were taken with a matched termination, and then with a matched piece of standard RG 5-U cable with type N connectors. The results of these measurements are shown in Fig. 19. The discontinuities present in the cable connections seemed sufficient to account for the variations in the standing-wave readings. The graph also introduces the problem of just how good a helix-to-coaxial junction is necessary. If standard cables and connectors are used, the results given in Fig. 19 impose a practical limit on the over-all performance. A practical coupling need not be better than this.

For this study, however, a precision coupling was desired for investigating the impedance presented by the helix with an external shield. An adaptor that would fit directly on the shield with a minimum of discontinuity was built for a type N connector. A cross section of the connector and entry into the shield is shown in Fig. 20. With this improved apparatus, standing-wave and phase measurements were made. From these measurements, VSWR plots were made as a function of frequency. In Fig. 21 these plots are given for the three shields used. Voltage-standing-wave ratios calculated from the theoretically determined impedances are superimposed for comparison.

These plots exhibit a periodicity, as the earlier plots did, but with the period considerably lengthened. The period now corresponds quite closely to a phase change of 360° in the much-shortened space between the type N connector and the solder joint to the helix. This confirms the idea, presented earlier, that the variations were caused by line resonances. The standing-wave ratio of the 0.610-inch (inside diameter) shield is quite good, and would be satisfactory for most purposes.

The standing-wave ratio of the smallest diameter shield, given in Fig. 21(c), is quite different from that predicted by the theory. From the theoretical impedance plot, one would expect a near match at the low frequency end, with a standing-wave ratio of about two at the high end. The actual plot varied erratically and gave a much greater mismatch at all frequencies. At present, this phenomenon has not been satisfactorily explained.

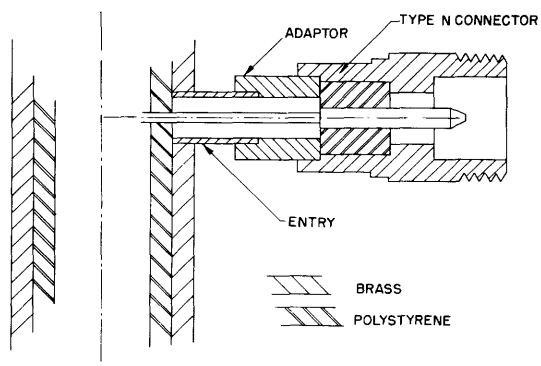

Fig. 20
Cross section of helix-to-coaxial-line coupling.

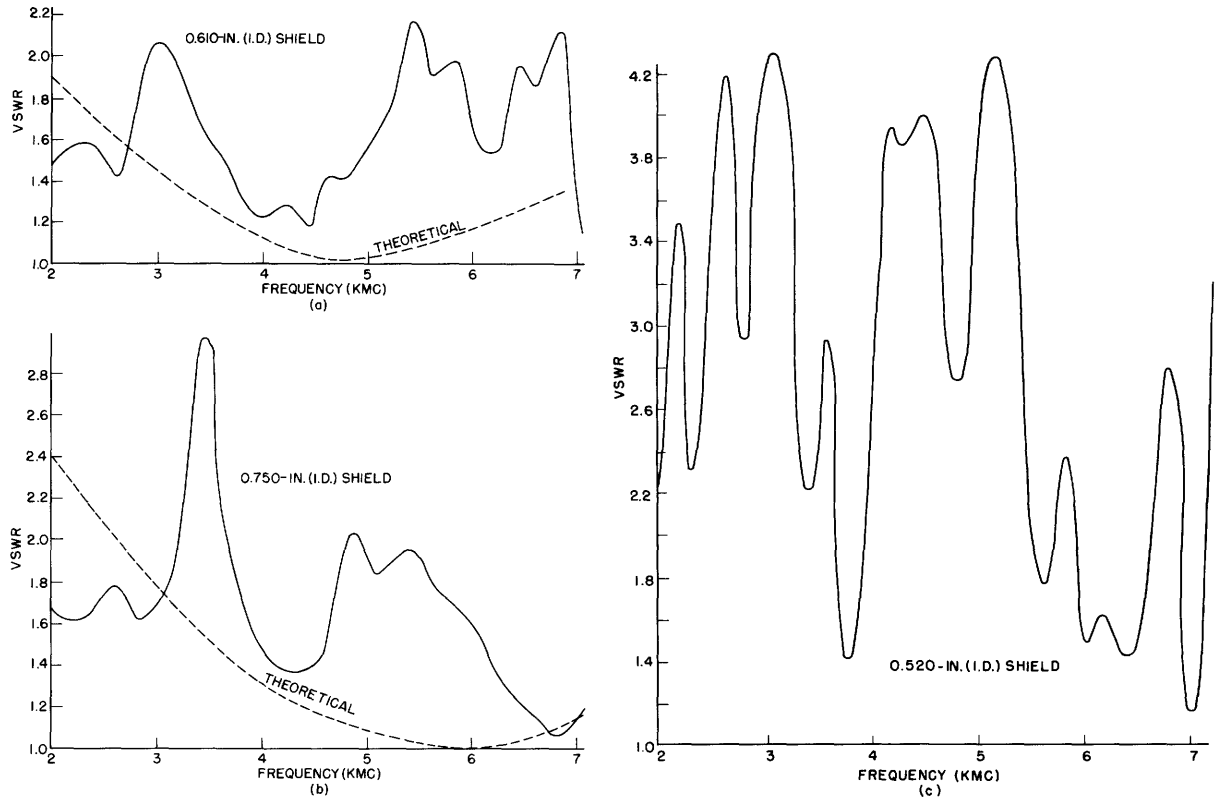

Fig. 21

Comparison of standing-wave ratios (coupling of Fig. 20): (a) 0.610-inch (I.D.) shield; (b) 0.750-inch (I.D.) shield; (c) 0.520-inch (I.D.) shield.

Smith-chart plots were also made of the impedances of the three structures, but because of the line resonances they did not yield much useful data. However, since the dips in standing-wave ratio should represent regions in which most of the reactive component had resonated out, careful plots in these regions should probably give a qualitative measure of Z_o. The results are tabulated in Table I and compared to the theory.

Table I

	0.750-inch (I.D.) shield		0.610-inch (I.D.) shield	
	Calculated	Experimental	Calculated	Experimental
2 kMc	119	95 + j0	92.5	90 - j20
4 kMc	69	55 + j30	58.5	50 + j0
7 kMc	41.8	55	36.4	55 + j25

2. THE COMPLETE COUPLING

In the preceding work, the individual problems of helix-to-helix and helix-to-coaxial transitions have been investigated. A complete coupling is simply a combination of

these two elements. A complete coupling that would fit on a backward-wave oscillator inside of an electromagnet is shown in Fig. 22.

The important properties of a helical coupling system for most applications are the percentage of the total power transferred and the directivity of the coupling. These two properties were used as a measure of the coupling performance. Power transfer was measured by the standing-wave techniques, with a VSWR of two, representing approximately a 10 per cent reflection of power. It was desired to achieve this over most of the region of interest, which was a three-to-one bandwidth from 2 kMc to 6 kMc.

Typical standing-wave and directivity patterns are given in Fig. 23. While these results still leave much to be desired, the given performance would probably be adequate for many wideband applications. Results could probably be improved by a more careful determination of parameters and an improved mechanical design. In fact, considerably better standing-wave ratios were achieved with one coupling, but results were not reproducible because of mechanical difficulties.

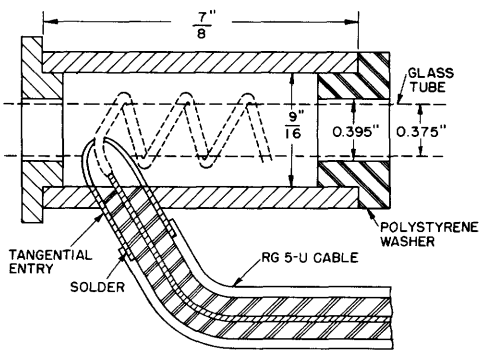

Fig. 22
A complete coupling.

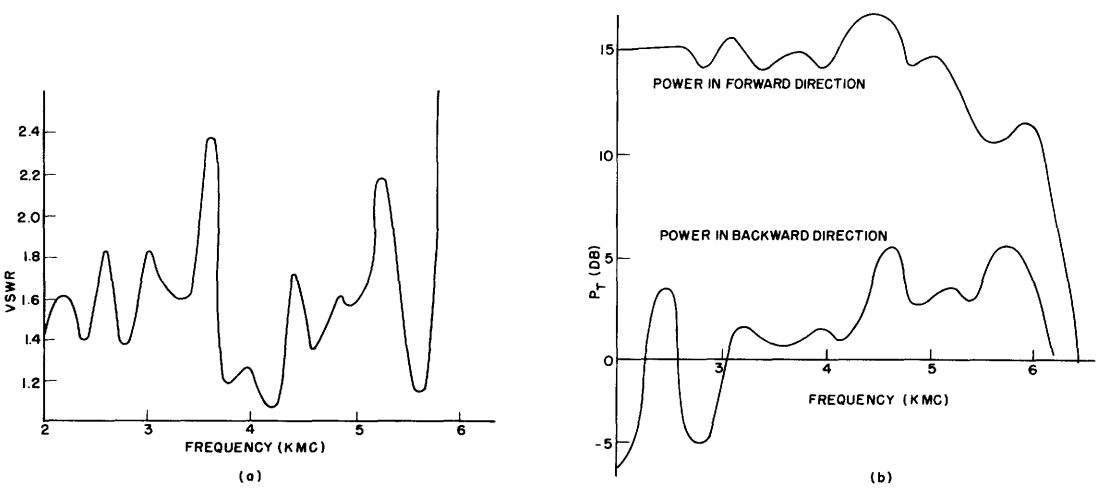

Fig. 23
Voltage-standing-wave ratios and directional properties of complete coupler.

APPENDIX I

EXPERIMENTAL METHODS

The experiments performed were:

1. Standing-wave measurements (impedance measurements).
2. Relative power measurements for coupling in forward and backward direction (directivity measurements).
3. Phase velocity measurements.
4. Beat wavelength measurements.

All measurements were "cold" measurements, performed without an electron stream or vacuum. The equipment and procedure employed in these experiments are given in detail below.

1. Standing-Wave Measurements

A block diagram of the experimental setup is shown in Fig. 24. For impedance measurements both standing-wave amplitude and phase were noted. A number of long shields (Fig. 25) of different inside diameters were built. Each of these had two inputs, one on each end of the shield, with inside diameters that would fit the dielectric of an RG 5-U cable. One of these inputs was for the perpendicular entry; the other, which was off center, was for the tangential entry. Either a standard cable or the special adaptor shown in Fig. 20 could be soldered to the inputs. Experiments were performed both with and without the dielectric sleeve between the shield and the helix. In either case, the central glass tube (representing the vacuum envelope) was present. The main helix, which would be inside the central glass envelope in a complete tube, was, of course, absent for these experiments. The outside diameter of the glass tube was somewhat smaller than the inside diameter of the helix. Because of this, the helix when supported by the outside dielectric sleeve was away from the glass and touched along one line when the sleeve was not used. This can be seen clearly from Fig. 25, which gives end views of the structure with the helices in place for the two cases. The center glass tube was given a graded coat of Aquadag to prevent reflections from the end of the helix. The Aquadag coat was never allowed to touch the helix.

The same standing-wave technique was used to measure the reflection from the complete coupling. For these measurements the shield, as shown in Fig. 22, extended only over the coupling helix. Power was fed into the coupling helix, which was unterminated. This power then coupled onto the inner helix, which had a matched termination. The matched termination was constructed by placing a graded Aquadag coating on the outside of the glass tube which separated the two helices. The entire termination was external to the coupling itself so that it would not interfere with the power transfer. The reflections that were noted by this arrangement were the totality of all reflections both from the helix-to-coaxial junction and those caused by the coupling between the two helices.

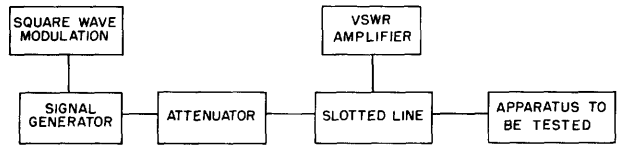

Fig. 24
Block diagram of VSWR measuring equipment.

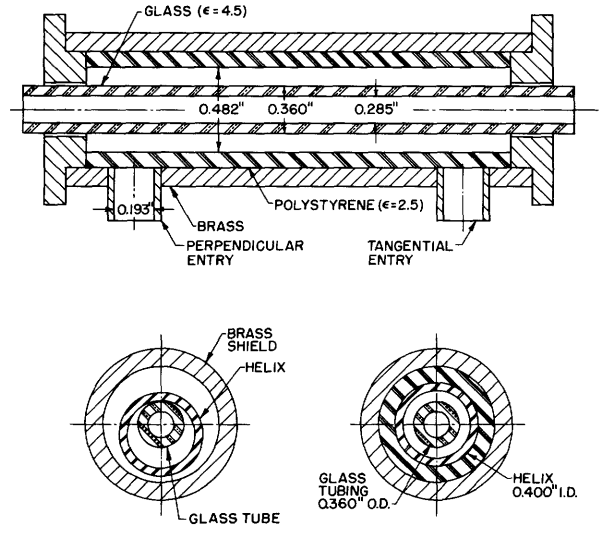

Fig. 25
Impedance measuring apparatus.

2. Directivity Measurements

The directivity measurements employed a setup very similar to that used for standing-wave measurements. Power was fed into the coupling helix and taken off one end of the inner helix; the other end of the inner helix was terminated in a matched load. By simply reversing the direction of the coupling in relation to the output and measuring the power out in both cases, a measure of the directivity of the coupling was obtained. In practice, a variable attenuator was used to keep the signal level at the detector constant so that the linearity of the detector need not be considered. The detector consisted of a matched slotted line from which the output power was sampled by a calibrated untuned probe and crystal. A block diagram is given in Fig. 26. Figure 27 shows the input and output coupling with the coupling helix in a position to measure power in the forward direction.

3. Phase Velocity Measurements

The accurate measurement of phase velocity has been previously shown to be of the utmost importance in the design of a good coupling. Various methods of measuring

phase velocities along a helix have been used with reasonable success. The method used for this work makes use of the properties of coupled helices that were being studied. If a quarter-wavelength of coupling helix is moved along a main helix, power will be transferred to the coupling helix and then reflected back again from the discontinuity at its end. If this discontinuity is then moved along the helix, the phase changes at the input can be noted on a standing-wave indicator. If the probe in the slotted line is kept at a fixed position, the distance between minima, measured in distance moved by the coupling helix, will give half-wavelengths along the helix. The longitudinal phase velocity is then simply a product of the helix wavelength and the frequency. All of the external environment of the coupling must, of course, be accurately reproduced in order to give the correct velocity. In Fig. 28 the complete measuring equipment is given, with the two probe helices shown separately. The phase velocity of the larger helix is being determined by the use of a small helix shorting probe. The variations of this method that can be used for measuring the velocities in other environments are fairly apparent.

4. Beat Wavelength Measurements

For measuring beat wavelengths, the same lathe setup was used as that used for measuring phase velocities. Two long helices representing the main and coupling helices were made to interact by sliding the smaller diameter helix concentrically into the larger. The farther ends of the two helices were connected to the signal source and the detector, respectively. As the interaction distance between the two helices changed, the amount of coupled power changed, maximum power coupling at an interaction distance of a quarter beat wavelength, and minimum power at a half beat wavelength. Since the minima were fairly sharp, as shown in Section I-1, it was quite easy to obtain a measure of the beat wavelength. As in the directivity measurements, the detector consisted of a matched slotted line with a calibrated crystal and probe. The output was held constant by a variable input attenuator from which the power transmitted could be read. The helices were supported in their concentric positions by various means, depending on the measurement wanted. To simulate the actual operational environment, a glass tube was used as the spacer. For measurements that

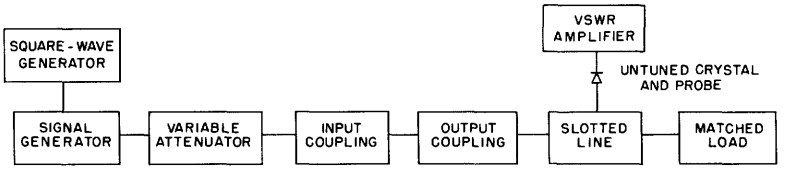

Fig. 26
Block diagram of directivity measuring equipment.

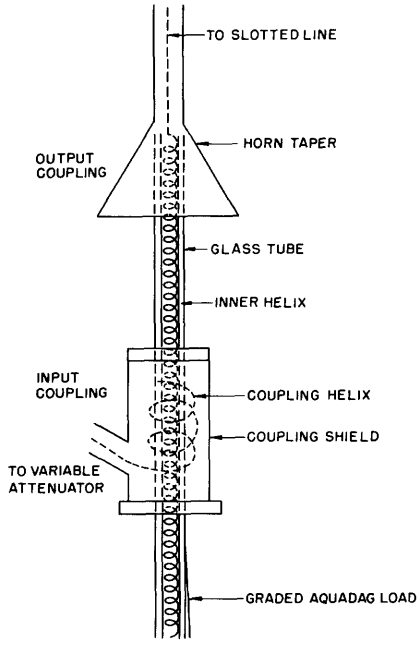

Fig. 27
Apparatus for directivity measurements.

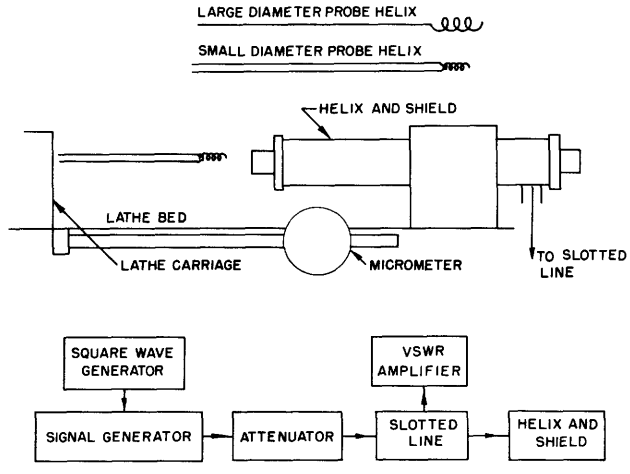

Fig. 28
Apparatus for phase velocity measurements.

would approximate free space interaction, in order to make theoretical comparisons, three teflon spacers were used. These were assumed to have very little effect on the wavelength, as was borne out in experiments by Smullin (9).

ACKNOWLEDGMENT

I would like to express my gratitude to Professor H. A. Haus and Mr. Louis Stark, with whom I have had many helpful discussions, and to Mr. L. D. Smullin, whose guidance and inspiration have been of inestimable value. Calculations were performed by Mida Karakashian.

REFERENCES

1. R. Kompfner, Traveling wave tubes, 38543, MM-53-150-8 Memorandum, Bell Telephone Laboratories, March 3, 1953.
2. J. R. Pierce, Traveling Wave Tubes, Chap. III (D. Van Nostrand Company, Inc., New York, 1950).
3. G. Wade, Propagation along coupled concentric helices, unpublished paper, Dec. 2, 1953.
4. A. J. Lichtenberg, A helical coupling system, M.Sc. Thesis, Department of Electrical Engineering, M.I.T. (1954).
5. P. D. Lacy, Applications of coupled helices, presented at the 1953 West Coast Convention of the Institute of Radio Engineers.
6. L. Stark, private communication.
7. G. W. C. Mathers and G. Kino, Some properties of a sheath helix with a center conductor or external shield, Technical Report 65, Electronics Research Laboratory, Stanford University, June 17, 1953.
8. S. Sensiper, Electromagnetic wave propagation on helical conductors, Technical Report 194, Research Laboratory of Electronics, M.I.T., May 16, 1951.
9. L. A. Harris, H. R. Johnson, A. Karp, and L. D. Smullin, Some measurements of phase velocity along a helix with dielectric supports, Technical Report 93, Research Laboratory of Electronics, M.I.T., Jan. 21, 1949.
10. H. S. Kirschbaum, The characteristic impedance and phase velocity of a shielded helical transmission line, Carnegie Institute of Technology.